Electronic Supplementary Information (ESI) for

Polypyrrole-coated manganese dioxide with multiscale architectures for ultrahigh capacity energy storage†

Jun Seop Lee[Ⅱ], **Dong Hoon Shin**[Ⅱ] **and Jyongsik Jang***

School of Chemical and Biological Engineering, College of Engineering, Seoul National University (SNU), 599 Gwanangno, Gwanak-gu, Seoul, 151-742 (Korea).

Fax: +82-2-888-7295; Tel: 82-2-880-8348; e-mail: jsjang@plaza.snu.ac.kr

1. XRD and XPS spectra of MnO_2 micronodules

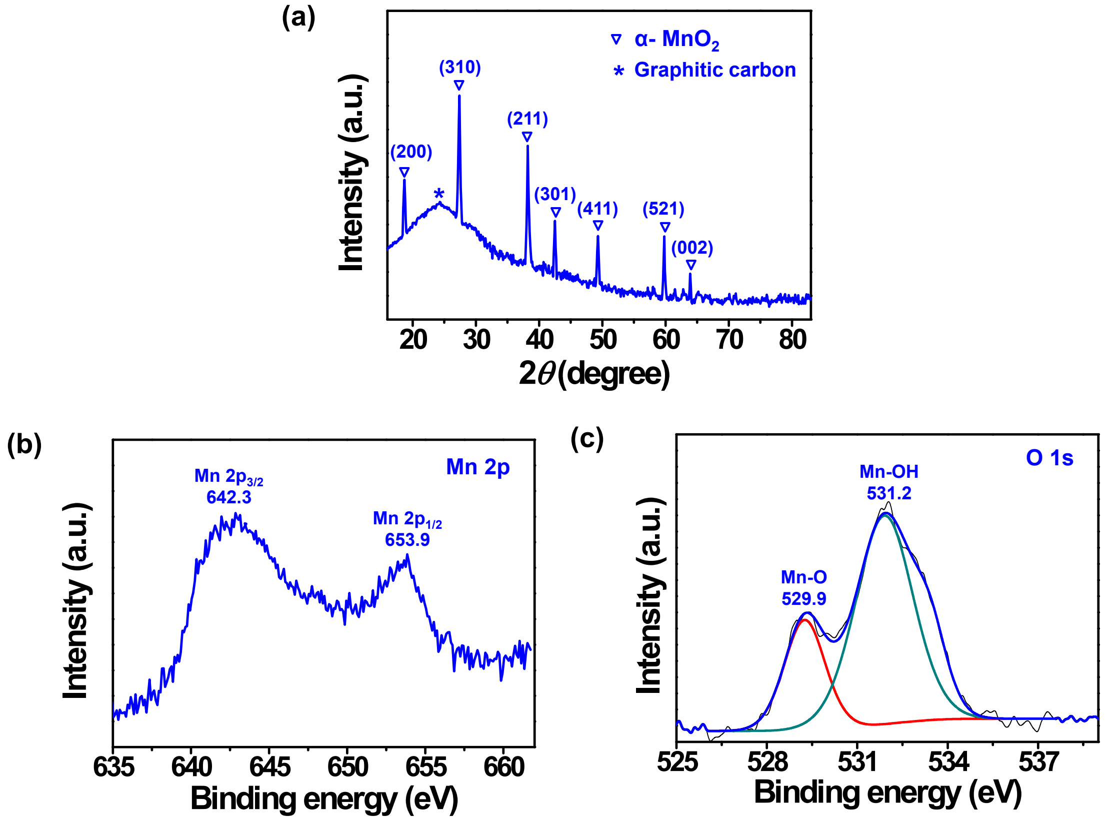

Figure S1. (a) X-ray diffraction (XRD) pattern and high-resolution X-ray photoelectron spectroscopy (XPS) spectra of (b) Mn 2p and (c) O 1s of MnO_2 micronodules on the carbon cloth.

The X-ray diffraction (XRD) pattern of the MnO_2 micronodules (MnO_2MNs) is shown in the **Figure S1a**. The peaks of the MnO_2MNs can be well indexed to tetragonal α-MnO_2 (JCPDS 44-0141). A broad diffraction peak at *ca.* 25.6 cm^{-1} was observed, indicating the identical crystalline carbon structure for the carbon cloth. The chemical composition of the micronodules was confirmed using X-ray photoelectron spectroscopy (XPS). **Figure S1b** shows the high-resolution XPS spectra for the Mn 2p peak. Spin-orbit Mn $2p_{1/2}$ and Mn $2p_{3/2}$ peaks were located at 642.3 and 653.9 eV, which is consistent with the reported values for MnO_2. Additionally, the O 1s spectrum can be deconvoluted into two components, suggesting the presence of two types of oxygen-containing species (**Figure S1c**). The bands at 529.9 eV and 531.2 eV were assigned to the oxygen bonds of Mn-O and Mn-OH, respectively.

2. MnO_2@PPy structure analysis

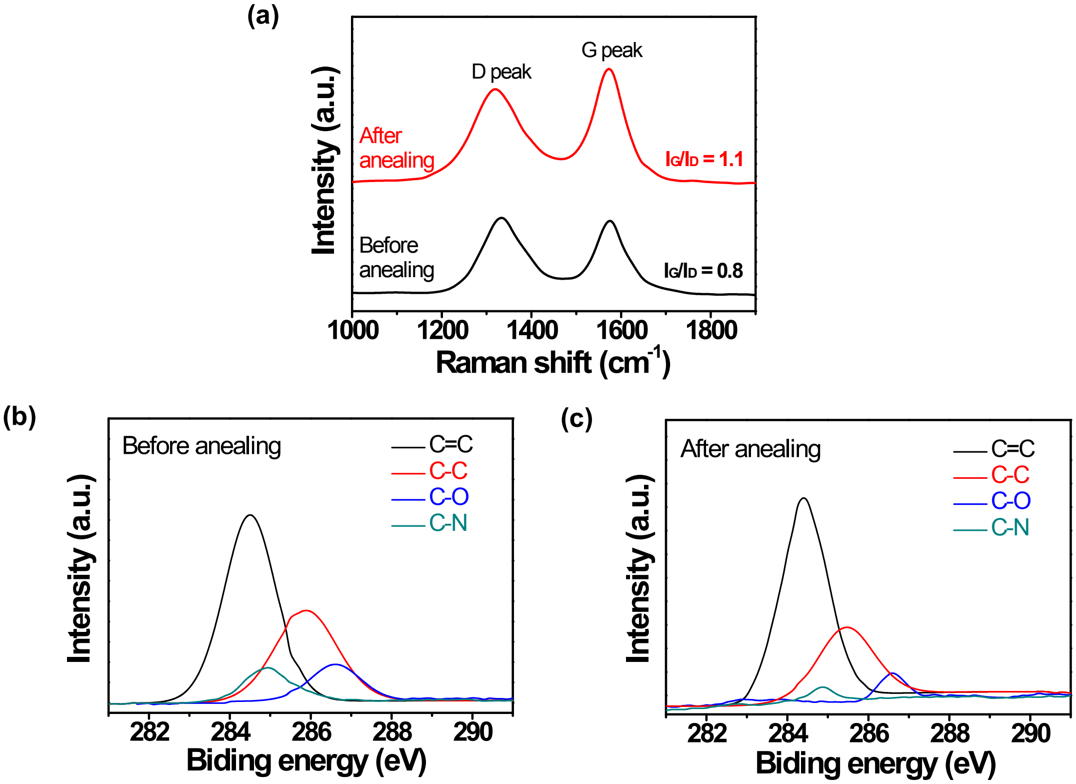

Figure S2. (a) Raman spectra of the MnO_2@PPy of before (black) and after (red) heat-annealing. High resolution XPS patterns of C 1s of (b) before and (c) after heat annealing of MnO_2@PPy**.**

To confirm the structure change of PPy layer, Raman and X-ray photoelectron spectroscopy (XPS) were conducted. First, Raman spectra were suggested as shown in **Figure S2a**. The I_G/I_D ratio of annealed MnO_2@PPy (~ 1.1) was higher than for without annealing (~ 0.8) and the peaks of after annealing were sharper than those of without annealing. In addition, X-ray photoelectron spectroscopy (XPS) of two materials was also suggested. The peaks of without annealed were attributed as follows: the 284.3 eV peak to C=C bonds, the 285.3 eV peak to C-C bonds, the 286.6 eV peak to C-O bonds, and the 284.9 eV peak to C-N bonds (**Figure S2b**). However, peaks of annealed MnO_2@PPy were changed as shown in **Figure S2c**. It displayed a large peak at 284.6 eV, which was attributed to graphitic sp^2 hybridization, and decreasing to additional peaks at 285.5 and 287.9 eV, which were assigned to C-O and C-N, respectively.

3. IR drop of various electrodes with different current density

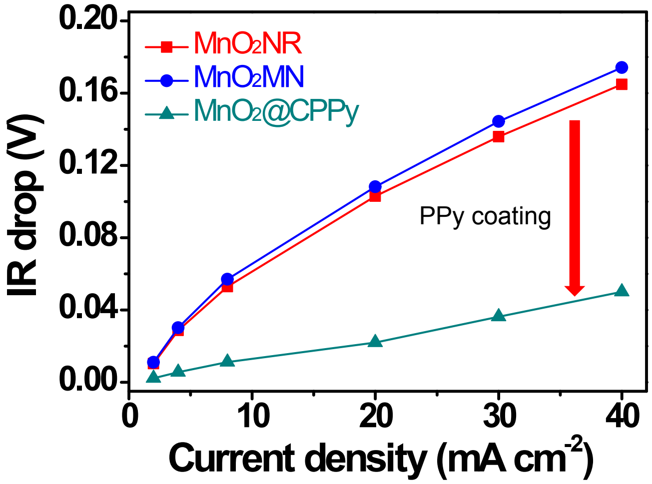

Figure S3. IR drop as a function of the current density of MnO_2NR (red)-, MnO_2MN (blue)- and MnO_2@CPPy (green)-based electrodes.

4. **Coulombic efficiency of various electrodes**

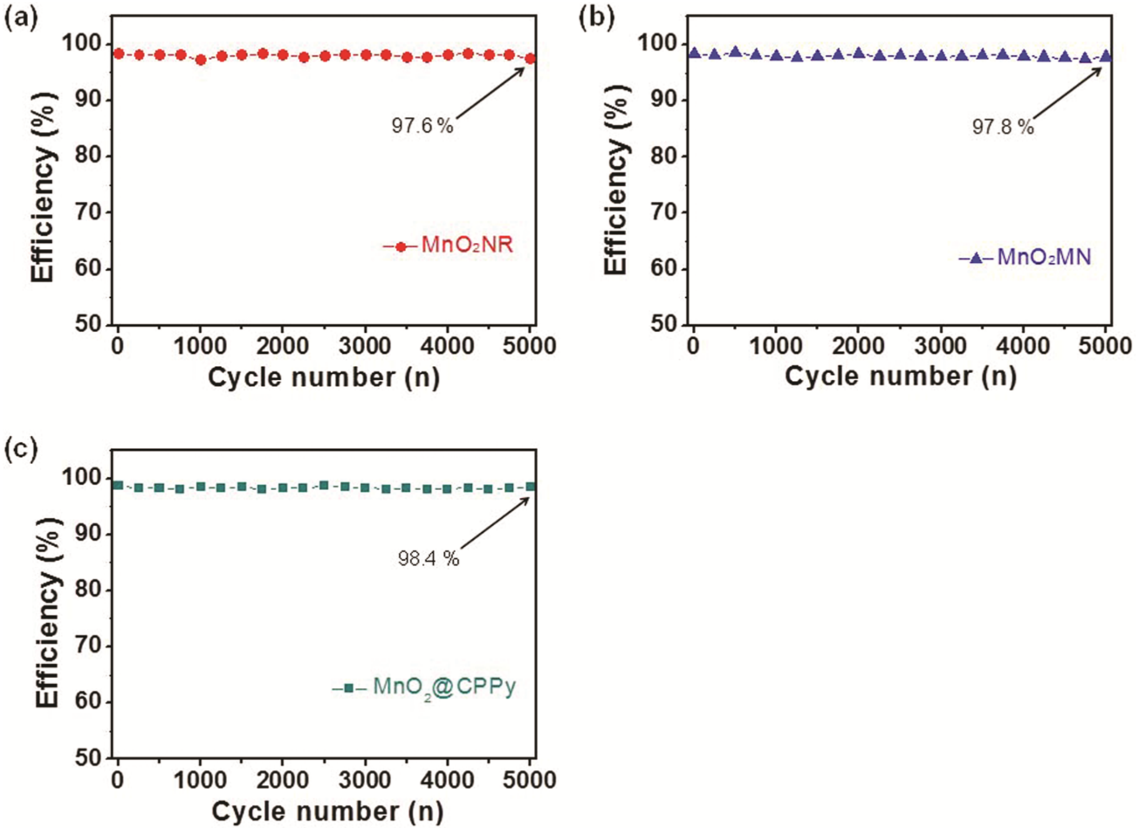

Figure S4. Coulombic efficiency of MnO_2-based electrodes at three-electrode systems with enhancing cycle numbers: (a) MnO_2NR; (b) MnO_2MN; (c) MnO_2@CPPy.

5. FE-SEM and TEM images of Co_3O_4@C architectures

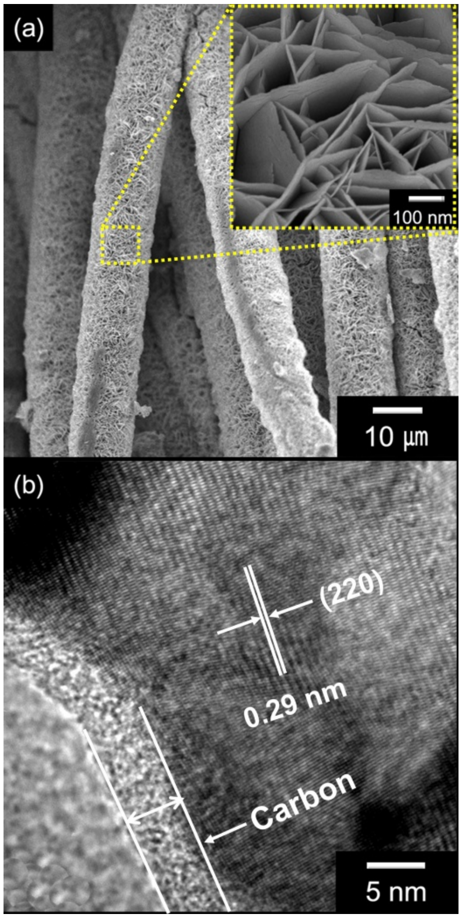

Figure S5. (a) Field effect scanning electron microscopy (FE-SEM) images of carbon coated Co_3O_4 (Co_3O_4@C) micro-sheet decorated carbon cloth (inset: enlarged image of Co_3O_4@C micro-sheets). (b) High-resolution transmission electron microscopy (HR-TEM) image of the Co_3O_4@C micro-sheet.

6. CV and galvanostatic charge/discharge curves of Co_3O_4@C electrode

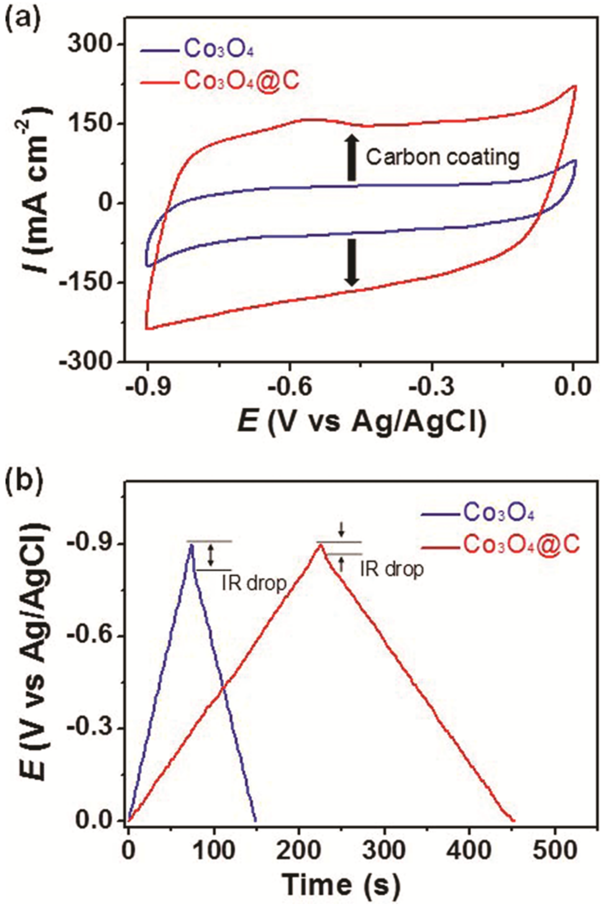

Figure S6. (a) Cyclic voltammetry (CV) (scan rate: 50 mV s^{-1}) and (b) galvanostatic charge-discharge curves (current density: 20 mA cm_{-2}) of the Co_3O_4-based electrodes.

Cyclic voltammetry (CV) of Co_3O_4 based electrodes (Co_3O_4 microsheet and Co_3O_4@C microsheet) were measured using three electrode cell composed of 1-M KOH aqueous electrolyte with Pt counter electrode and Ag/AgCl reference electrode. The CV curves of the electrodes were conducted at scan rate of 50 mV s^{-1} over the voltage range -0.9 to 0 V. As shown in **Figure S6a**, the current density of Co_3O_4@C microsheet was 221.3 mA cm^{-2} that was *ca*. 3-fold larger than that of Co_3O_4 microsheet electrode (72.3 mA cm^{-2}) due to carbon coating layer enhanced electrochemical activity of the active materials at negative voltage range.[S1] Galvanostatic charge-discharge curve of the electrodes were also carried out at 20 mA cm^{-2} of current density as shown in **Figure S6b**. The discharge time also rapidly increased with carbon coating on the Co_3O_4 surface (Co_3O_4 microsheet: 74.3 s and Co_3O_4@C microsheet: 232.2 s). Additionally, IR drop of the electrodes decreased with carbon coating layer (0.1 V to 0.03 V) owing to carbon also acted as conductive layer in the electrode structure.

[S1] X. Lu, M. Yu, G. Wang, T. Zhai, S. Xie, Y. Ling, Y. Tong and Y. Li, *Adv. Mater*. **2013**, *25*, 267.

7. Schematic diagram and photograph image of ASCs

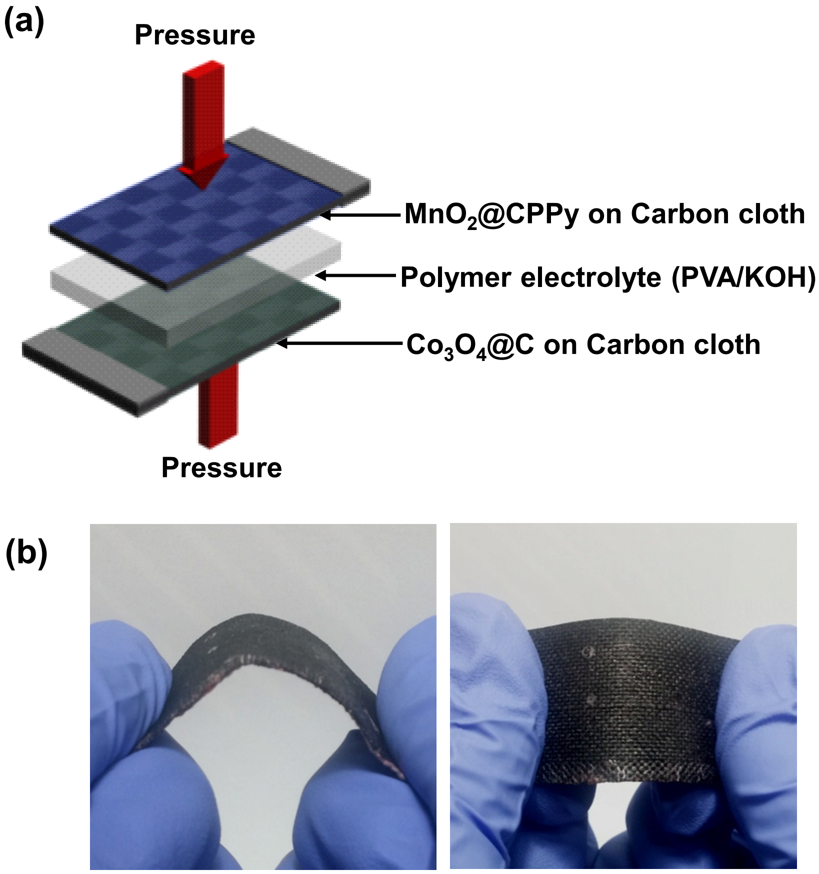

Figure S7. (a) Schematic diagram of asymmetric supercapacitors (ASCs) composed of two different electrodes (MnO_2@CPPy: positive; Co_3O_4@C: negative) and a polymer-gel electrolyte. (b) Two digital photographs (front and side directions) of bend ASCs.

8. Bode plot of ASC

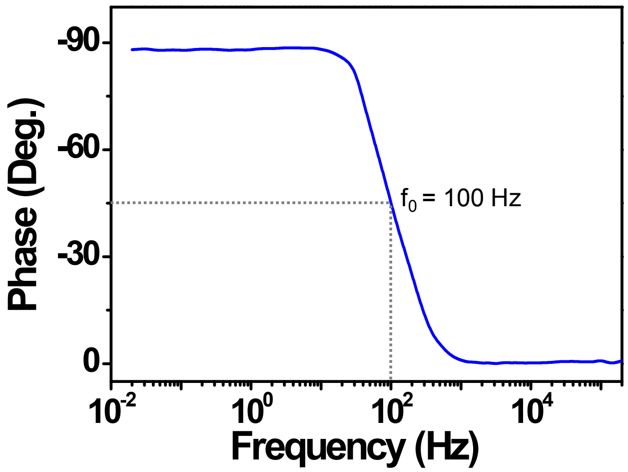

Figure S8. Bode phase plot of the ASCs (frequency: 200 kHz to 20 mHz).

9. Other specific capacitance variation of ASC with different current density

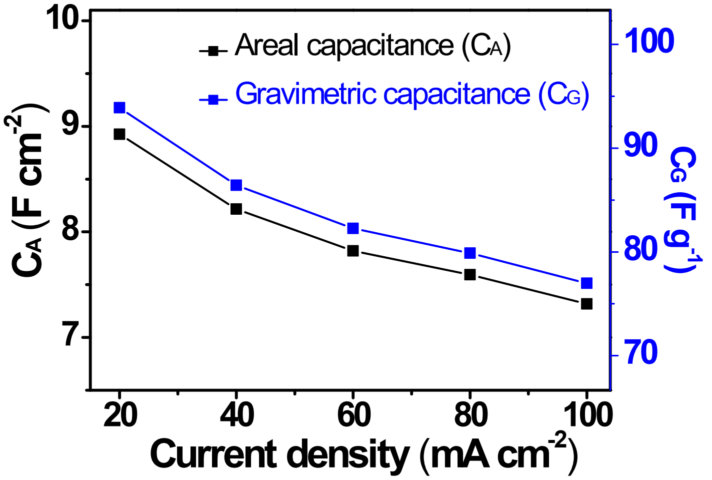

Figure S9. Areal (C_A) and gravimetric (C_G) capacitance of the ASCs with different current densities (20 to 100 mA cm^{-2}).

10. Coulombic efficiency of ASC

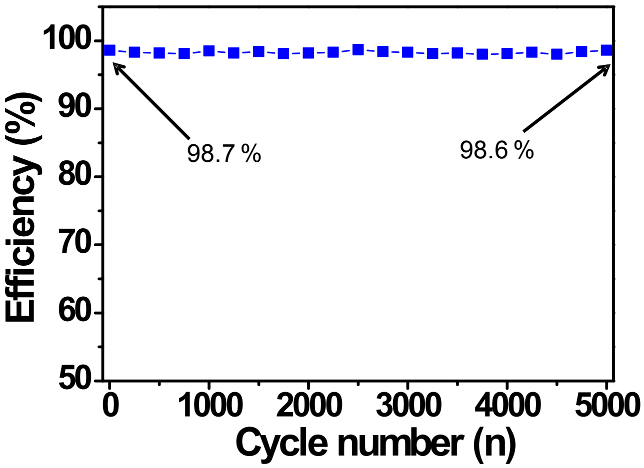

Figure S10. Coulombic efficiency of the ASCs with increasing cycle numbers.